ISSN: 2634-9221
European Journal of Applied Sciences; Vol. 14 No. 03 (2026) (467-490)
https://doi.org/10.14738/ejas.1403.11886

Green Chemistry Preparation of *Canarium schweinfurthii* Activated Carbon/Silver Nanoparticle Composite as Effective Antibacterial Agent for Bacterial Polluted Water Treatment

Gadjui Youatou Boris[1], Ankoro Naphtali Odogu[1,2,3*], Kouotou Daouda[1*], Lunga Paul Keilah[2], Ndi Julius Nsami[1], Ngomo Horace Manga[1] and Ketcha Joseph Mbadcam[1]

1. Applied Physical and Analytical Chemistry Laboratory, Department of Inorganic Chemistry, Faculty of Science, University of Yaoundé I, PO. Box 812, Yaoundé, Cameroon
2. Antimicrobial and Biocontrol Agents Unit (AmBcAU), Laboratory for Phytobiochemistry and Medicinal Plants Studies, Department of Biochemistry, Faculty of Science, University of Yaounde´ I, P.O. Box 812, Yaounde´, Cameroon
3. Department of Chemistry, Faculty of Science, University of Buea, Buea, PO Box 63, Cameroon

Abstract: Targeting contaminated water containing dye and bacteria is primordial to humans. The adsorption technique has been efficient, but an added antibacterial proper is prime to modern-day functioning. Silver nanoparticles provide an excellent platform for biological and material applications due to their unique physical and chemical properties. Three potential materials were prepared namely *Canarium schweinfurthii* activated carbon (CSAC), Silver nanoparticles (AgNP) and *Canarium schweinfurthii* activated carbon/Silver nanoparticles (CSAC/AgNP). *Canarium schweinfurthii (*CS) precursors were subjected to thermogravimetric analysis (TGA), CSAC material was characterized by scanning electron microscopy-energy dispersive spectrometry (SEM-EDS), X-ray fluorescence (XRF), Fourier transformed infrared spectroscopy (FT-IR) and nitrogen adsorption/desorption (N_2-BET) and the AgNP was investigated using UV-Visible analysis. The UV-visible analysis of the nanoparticle shows a strong surface Plasmon resonance peak at 471 nm; the CSAC sample presented high methyl orange (MO) dye uptake varying from 48.293 to 98.328 mg/g. CSAC sample and the extract gave no antimicrobial properties while AgNP and CSAC/AgNP samples exhibited strong antibacterial activities while AgNP had a bactericidal effect on the six bacteria isolates of EC ATCC25922: *Escherichia coli* ATCC25922; SA ATCC43300: *Staphylococcus aureus* ATCC 43300; SANR 46003: *Staphylococcus aureus* NR 46003; S.cho NR-170: *Salmonella choleriesus* NR-170; SENR 13555: *Salmonella enteritica* 13555; SENR 4811: *Salmonella enteritica* 4811.

Keywords: *Canarium schweinfurthii*, Activated carbon, Silver Nanoparticle, Bacterial Isolate, Adsorption, Wastewaters.

INTRODUCTION

Water shortage is a growing global problem that is not restricted to the developing world [1]. Water scarcity is already present on every continent, and the demand for water has been growing globally at more than twice the rate of population increase over the last century [2]. According to the United Nations Educational, Scientific and Cultural Organization (UNESCO), the world population is predicted to increase by 33% between 2011 and 2050, growing from 7.0 billion to 9.3 billion [3]. By 2025, approximately 1.8 billion people are anticipated to be living in areas with absolute water scarcity, and two-thirds of the world population is expected to be living under conditions of water stress, further

emphasizing the need for more effective water and wastewater treatment and management [3-4].

Dyes are widely used in various industries such as textiles, paint, tanneries, plastics, rubber, pharmacies, electroplating, and food processing, and discharge of wastewater from these industries without proper treatment will result in severe environmental problems to aquatic animals and human beings [5-6]. These effluents are usually effective side for bacterial growth and replication. Bacterial infections are considered a major threat to public health [7]. The most effective treatment for pathogenic bacteria in the medical system is the use of antibiotics. The limitation of antibiotics is that some antibiotics only have antibacterial effects against a certain type of pathogenic bacteria, and do not have broad-spectrum antibacterial properties [8]. Development of multi-drug resistance (MDR) in bacterial strains, including Enterococci, Staphylococci, Klebsiella, Acinetobacter, Pseudomonas, Enterobacter species, etc., has become a severe challenge [9-10].

These bacteria are displaying resistance to world-leading antibiotics, including Cephalosporins, Carbapenems, Vancomycin, and Methicillin [11]. According to the World Health Organization (WHO), current deaths due to microbial diseases are ~0.7 million per year; if we could not develop efficient drugs to control or destroy these pathogenic microbes, the deaths caused by microbial diseases may rise to ~10 million by 2050 [12]. Due to the rapid emergence of antibiotic-resistant strains, it has become obligatory to find alternatives to antibiotics or routes to tackle these MDR pathogenic microbes and dyes from wastewater [12]. To prevent dyes such as methyl orange and bacterial from reaching drinking or surrounding water, several methods, including thermal degradation using non-thermic plasma, electrocoagulation, reverse osmosis and adsorption, have been developed [14-15]. Among the above-cited methods, the adsorption technique is promising based on its economic aspect, flexibility, simplicity of design and ability to remove various pollutants even at low concentrations [16-17]. However, various adsorbents, including carbon-based materials, chitosan, clay, volcanic pumice and zeolite, have been successfully used for methylene blue dye removal [18,19,20 ;21]. For industrial water treatment, activated carbons are so far considered the best adsorbent due to their various type of surface functional groups, well-developed pore structure, high porosity and large surface area which make them called versatile materials [18, 22, 23]. Activated carbon has high adsorptive capacity with respect to dyes, but the presence of bacteria creates biofilm, which distorts its efficiency. Hence preparation of activated carbon with antibacterial properties is of prime priority.

Recently, the preparation of materials with high antibacterial activity has broad prospective applications. Silver nanoparticles have been widely used in the preparation of antibacterial materials for the treatment of bacteria and pathogens [24]. These nanoparticles have been widely prepared through chemical means with the help of solvents like ethanol, methanol, ether, etc, as a capping and reducing agent [9]. These solvents are considered toxic to humans, and therefore, a new synthetic route is badly required. Nowadays, green chemistry has drawn wide attention from scholars in the preparation of nanoparticles due to their simple synthesis, low toxicity, good biocompatibility and easy surface modification [25]. Moreover, the bactericidal activity of AgNPs is dependent on the chemistry and size of their surface [26]. It is believed that, for activated carbon doped with AgNP, electrostatic interaction mainly contributes to their antibacterial properties and shows size-dependent growth inhibition of bacteria, which may contribute to the

destruction of bacterial membranes via high positive charges [12]. They also effectively inhibited the formation of bacterial biofilms without drug resistance [27]. Furthermore, numerous studies have demonstrated that the synergistic effect of AgNPs with other materials can enhance antibacterial activity, while also efficiently decreasing the size and preventing the aggregation of the AgNPs [25]. This enhancement can be done without destroying the potential function of the material. Finding suitable surface passivation or support materials for silver nanoparticles can retain their antibacterial activity while having better stability, which can solve the above problem and perform other functions, is also a major target [11].

Nanocomposites can be composited with silver nanoparticles and activated carbon for a more rational design, which combines the Physico chemical properties of activated carbon and the biological properties of AgNPs [12]. In this work, we modified the CSAC by depositing Ag nanoparticles on the surface of the carbon, which promised two advantages: (a) to prevent aggregation of AgNPs and (b) to have high adsorption capacity CSAC. These properties make the composite suitable for potential improvement in the treatment of wastewater and wastewater-containing pathogens. The AgNPs/CSAC composite were synthesized through a one-step synthetic process and their adsorption and antibacterial properties were systematically investigated. The as-synthesized composite showed excellent antibacterial properties against Gram-negative/Gram-positive bacteria and fungi.

MATERIALS AND METHODS

Sampling of Precursors and Preparation of Activated Carbon Adsorbent

The sampling of *Canarium schweinfurthii* seeds was done in some markets in the West region of Cameroon. They were first washed abundantly with tap water to remove all dirties, followed by washing with distilled water and drying. The seeds were ground and sieved at the particle sizes ranging from 1.0-2.0 mm. The sieved sample was mixed with phosphoric acid (orthophosphoric acid, 85% of purity from PA Panreac, used without any further purification) in a ratio of 1:1. The resulting mixture was stirred for 1.0 h and oven-dried for 24 h at 110°C then allowed to cool in a desiccator and finally carbonized at 600°C at the heating rate of 10°C. The obtained charred was washed with distilled water to neutral pH, dried, grinned and sieved to a size less than 75 µm, and the sample was named CSAC.

Preparation of Silver Nanoparticles and Nanocomposite

Preparation of Silver Nanoparticles

10.0 g of the *Canarium schweinfurthii* powder was mixed with 500 mL of distilled water and stirred using a magnetic stirrer for 1H; the resulting solution was filtered. In 100 mL of 5 mM nitrate ($AgNO_3$) solution, 100 mL of filtrate was added slowly and observed for colour change. The resulting particles obtained from the reduction of $AgNO_3$ were called AgNP.

Preparation of Silver Nanocomposite

The AgNP was loaded on AC by means of simple precipitation, as depicted by [17] with some modifications. Precisely, 5.0 g of the CSAC was added to the obtained AgNP solution; the

mixture was mixed vigorously by continuous stirring for 1h 30 min at 150 rpm using a horseshoe IKA agitator. It was allowed to settle, and the clear liquid was taped off. The nanocomposite solid obtained was dried in an oven at 110°C. The resulting sample was named CSAC/AgNP.

Samples Characterization

The thermogravimetric analysis (TGA) and differential scanning colourimetry (DSC) of CS seeds were evaluated using a thermogravimetric analyzer, TGA/DSC (LENSEIS STAPT-1000 thermal analyzer). The surface morphologies of CS precursor and CSAC materials were observed using a Scanning Electron Microscopy equipped with an Energy Dispersive Spectrometer (SEM/EDS, LEO 1455 VP). The X-ray fluorescence spectrometry (PANalytical X' Pert Pro) of CS and CSAC was carried out. The FT-IR measurements were also carried out in the absorbance mode ranging from 400 to 4000 cm^{-1} using Universal ATR, Crystal: Platinum, Diamond, Bounces: 1, and Solvent: ethanol for surface functional groups determination. The pore structure and surface area of the CSAC were done using nitrogen adsorption/desorption at -196°C, which was conducted using a gas sorption analyzer, Quantachrome, NOVA 1000 series, USA. The UV-visible spectrum of synthesized AgNPs was analyzed by using himadzu UV-visible spectrophotometer (UV-1800, Japan) ranging from 300 to 1100 nm.

Batch Adsorption Experiments

Batch adsorption experiments were carried out by mechanical agitation at room temperature (27± 0.1) °C. For each run, 20.0 mL of MO_{dye} of known initial concentration was treated with a known mass of CSAC adsorbent. After agitation using Multipurpose Flask Shaker TT12F from Techmel and Techmel USA at a speed of 160 rpm for a fixed period of time. The solution was filtered using the Whatman number 1 filter, and the filtrate was subsequently analyzed for Methyl orange (MO) residual concentration by UV/Vis spectrophotometer, model S23A from Techmel and Techmel USA at a wavelength of 464 nm. Similar measurements were also carried out for various CSAC doses (0.01 to 0.06 g), pH (2 to 10) and initial concentration of MO solution (50 to 100 mg/L). The MO_{dye} amount adsorbed per unit mass of adsorbent at equilibrium Q_e (mg/g) was calculated by using the following expression.

$$Q_e = \frac{(C_O - C_e)}{m} \times V \quad (1)$$

$$Q_t = \frac{(C_O - C_t)}{m} \times V \quad (2)$$

where Co, Ce, and Ct (in mg/L) are the initial equilibrium and concentration at the time, t, of the MO solution, respectively, m (g) is the mass of the adsorbent, and V (L) is the volume of the solution.

Non-linear Adsorption Isotherms and Kinetic Modelling of the Adsorption Data

Adsorption Isotherm Studies

Three non-linear adsorption isotherms, Langmuir, Freundlich and Temkin isotherms, were used to analyze the experimental data and their non-linear forms (Lekene et al., 2021). The respective isotherms equations models used are given below.

$$q_e = \frac{q_m K_L C_e}{1+K_L C_e} \quad [16]$$

$$q_e = K_F C_e^{\frac{1}{n}} \quad [21]$$

$$q_e = \frac{RT}{b}\ln(K_T C_e) \quad [17]$$

Where C_e (mg/L) and q_e (mg/g) are the concentration and the adsorbed quantity of MO dye at equilibrium, q_m is the maximum adsorbed quantity, K_L (L/mg) is the Langmuir adsorption constant, K_F ((mg/g)(L/mg)$^{1/n}$) is the Freundlich adsorption constant related to adsorption capacity, n is the energetic heterogeneity of surface, K_T is the equilibrium binding constant (L.mg^{-1}) corresponding to the maximum binding energy and constant b (J/mol) is related to the heat of adsorption, K (mol^2.k/J) is a constant related to the adsorption energy. R (8.314 J/mol. K) is the perfect gas constant and T (K) is the temperature at which the adsorption took place.

Kinetics Studies

To describe the mechanism of the adsorption process and the rate-controlling step of MO onto CSAC adsorbents, four kinetic models, pseudo-first-order, pseudo-second-order, Elovich, and intraparticle diffusion, were used to correlate the experimental data and their non-linear forms (). The respective kinetic equation models used are given below.

$$q_t = q_e[1 - \exp(-k_1 t)] \quad [18]$$

$$q_t = \frac{q_e^2 k_2 t}{1+q_e k_2 t} \quad [17]$$

$$q_t = \frac{1}{\beta}\ln(1 + \alpha\beta t) \quad [17]$$

$$q_t = k_i t^2 + C_i \quad [28]$$

Where qt and qe (mg/g) are the adsorbed quantity at a given time, t and equilibrium, respectively. K_1 (min^{-1}), K_2 (g/mg.min), and ki (mg/g.min-0.5) are the rate constants of pseudo-first-order, pseudo-second-order and intra-particle diffusion models, respectively. α (mg. g/min) is the rate of the initial adsorption, ß (g/mg) is the desorption constant and C_i is a constant value depicting the boundary layer effect.

The validity of the different aforementioned models was evaluated using correlation coefficient (R^2), root mean square error (*RMSE*) and Chi-square test (x^2) [28]. The respective relations are given below:

$$R^2 = 1 - \frac{\sum_{n=1}^{n}(q_{e.\exp,n} - q_{e.pre,n})^2}{\sum_{n=1}^{n}(q_{e.\exp,n} - \overline{q_{e.\exp,n}})^2} \quad [29]$$

$$RMSE = \sqrt{\frac{\sum_{n=1}^{n}(q_{e.exp,n} - q_{e.pre,n})^2}{n-1}}$$

$$\chi^2 = \sum_{n=1}^{n} \frac{(q_{e.exp,n} - q_{e.pre,n})^2}{q_{e.exp,n}}$$

Evaluation of Antibacterial Properties

The in-vitro antibacterial activity of the extracts was evaluated on six bacteria isolates of EC ATCC25922: *Escherichia coli* ATCC25922; SA ATCC43300: *Staphylococcus aureus* ATCC 43300; SANR 46003: *Staphylococcus aureus* NR 46003; S.cho NR-170: *Salmonella choleriesus* NR-170; SENR 13555: *Salmonella enteritica* 13555; SENR 4811: *Salmonella enteritica* 4811 gotten from the "Centre Hospitalier Universitaire" (CHU) of Yaounde-Cameroon. The minimum inhibitory concentration (MIC) and minimum Bacteria concentration (MBC) of the Shell extract, CSAC, AgNP and CSAC/AgNP were determined by the broth microdilution method, using a p-donitrotetrazolium chloride (INT) based assay as previously reported by Lunga et al. (2014) with some modifications. Briefly, 196 mL of Muller Hinton broth (MHB) was introduced into the wells of the first line, followed by 4mL of each sample (initially prepared at 100 mg/mL in 100% DMSO). Serial two-fold dilutions were performed, and 100mL of the bacterial suspension (1.5*106 CFU/mL) was added. The final concentration ranged from 500 to 1.953 mg/mL for the samples and from 5 to 0.0195 mg/mL for the positive control (Ciprofloxacin). The plates were incubated at 37°C for 24 h after which 50 mL of 0.2 mg/mL INT solution was added and further incubated at 37°C for 30 min. MICs were determined as the lowest sample concentration with no visible colour change. Wells containing MHB and bacteria constituted the negative control while the sterility control contained MHB alone. The final concentration of DMSO was at most 1% and the preliminary test did not inhibit bacterial growth.

RESULTS AND DISCUSSION

Characterization of CS, CSAC and AgNP Samples

X-ray Fluorescence Analysis of CS and CSAC Materials

The metallic elements present in our different samples were highlighted by the X-ray fluorescence analysis method. Figure 1 shows the spectra of the results for the different materials in the different samples.

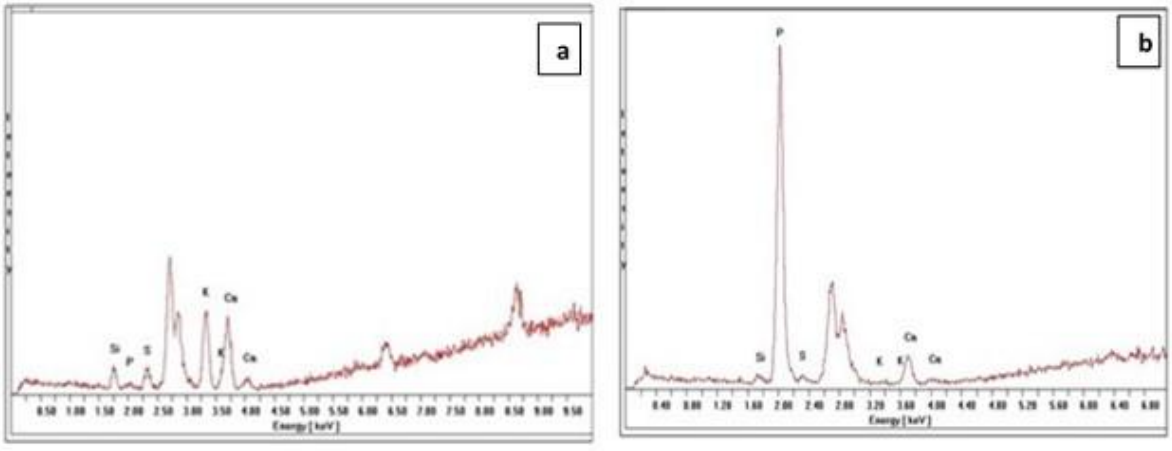

Figure 1: spectre de la fluorescence X de (a) CS and (b) CSAC

According to Figure 1, the peaks appearing at 2.7 keV correspond to the existence of the metal Rh due to the characteristics of the spectrometer tube, i.e. the fluorescence is caused by the material of the anode. Indeed, rhodium is used in some X-ray tubes, on their anodes, especially in the field of X-ray fluorescence spectrometry. Therefore, should not be taken into account when interpreting the spectra of all materials. Figure 1 (a) shows the spectra of the raw *Canarium schweinfurthii*. According to this spectrum, the different elements that enter the composition of the CS are potassium (K), calcium (Ca), sulfur (S), silicon (Si) and phosphorus (P). It is also observed that the major elements are potassium (K) and calcium (Ca) while the other spectra present are in trace amounts. In Figure 1 (b) the spectra of CSAC carbon, it is noted that the elements that enter the majority in their composition are among others calcium (Ca), sulfur (S), silicon (Si), phosphorus (P) and potassium (K) which concerns the spectrum of Figure 1 (d). Moreover, these spectra also show that the major element present in these materials is phosphorus (P) while the others are in trace states. The absence of the element potassium or its presence in trace amounts (very small quantities) of the carbon may result from the fact that during the activation of the latter with phosphoric acid, the potassium reacted with the phosphoric acid to form potassium phosphate, which is soluble in water. This potassium phosphate was, therefore, leached out during the washing of the latter, hence its absence or its presence in a very low concentration. These effects can be shown by the following equation:

$$K^+ + \quad H_3PO_4 \rightarrow \quad K_3PO_4 + \quad H^+ \quad \ldots\ldots\ldots\ldots\ldots\ldots\ldots\ldots\ldots\ldots (13)$$

Thermogravimetric Analysis of Canarium schweinfurthii (CS) Precursors

To study the thermochemical behaviours and observe the phenomena involved during the pyrolysis of the two biomasses used raw, we studied them by thermogravimetric and differential analysis (TGA, DTG, and DTA). The aim was to record the mass losses and analyze the variations of mass and temperature as a function of time. Figure 2 shows the thermogram of our precursor (CS).

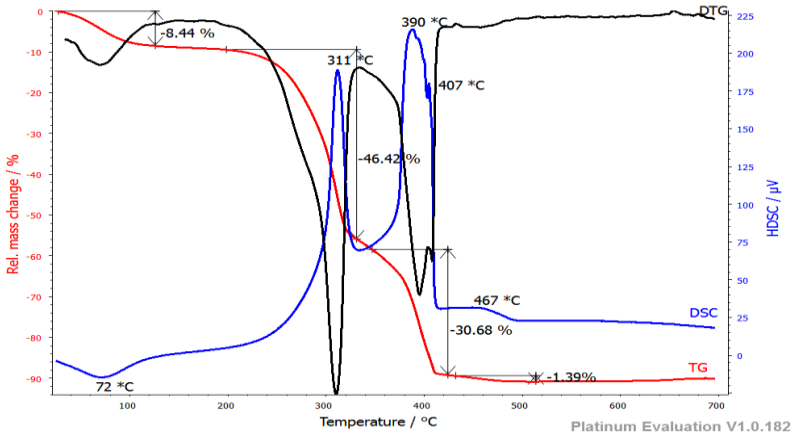

Figure 2: Thermogravimetric analysis of *Canarium schweinfurthii*

Figure 2 portrays four thermal accidents. The first one appears at 72°C, corresponding to the departure of free water at the surface of the material with a weight loss of approximately 8.44%, which is an endothermic process.

The second thermal accident occurs around 311°C, resulting in a loss of mass of about 46.42%. This loss of mass could be attributed to the degradation of hemicellulose, and the phenomenon is exothermic.

The third thermal accident appearing around 390°C corresponds to a loss of mass of 30.68%. This is the degradation of cellulose followed by the beginning of the degradation of lignin.

The fourth thermal accident, which, appears between 400 and 520°C, corresponds to the total decomposition of lignin with a loss of mass of 1.39%. This is also the low level of lignin in the precursor.

These results are in agreement with the work of K. Raveendran et al. (1995), who show that cellulose decomposes in a narrow temperature range (300°C −400°C and 325°C −375°C) while lignin dissociates in a much wider temperature zone (250°C −550°C and 200°C −500 C°). The authors also indicate that hemicelluloses, the least thermally stable compounds, decompose at rather low temperatures in the range of 200-250°C.

Above 520°C, the bonds rupture, allowing volatile matter to depart. Thus, only ash (inorganic matter) remains. Consequently, the carbonization temperature was chosen between 400 and 600°C.

FTIP Spectral of CS and CSAC Samples

The characterization of the precursors and the composite materials by Fourier Transform Infrared spectroscopy allows the identification of the different functional groups on the surface of the materials. The identification of the functional groups on the surface of the different activated carbons could better allow us to explain why some molecules are more adsorbed than others. The fact that a surface is formed of a high rate of acid or basic functions, favors or disadvantages the adsorption of such or such other molecule.

The infrared spectra of activated carbons prepared from impregnated CS and CSAC are given in Figure 3.

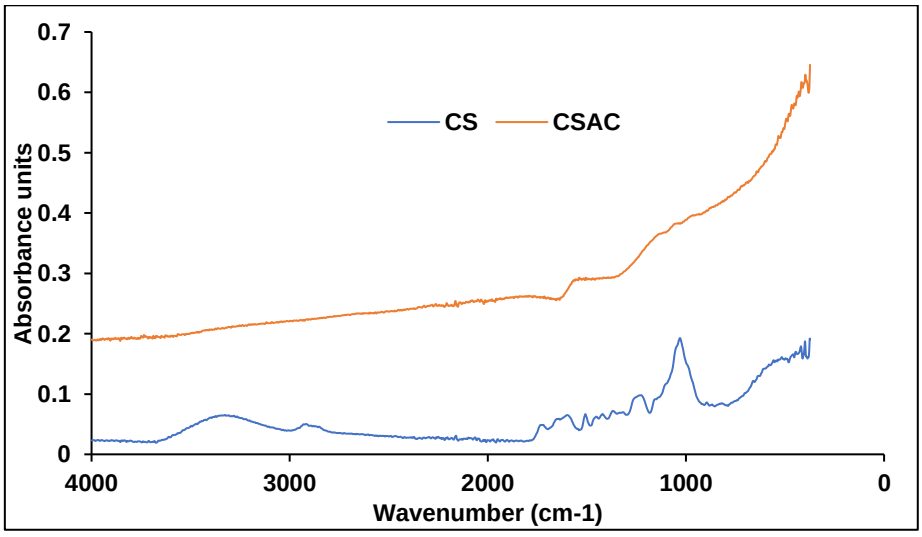

Figure 3: IR spectrum of the raw biomass (CS) and CSAC

It can be seen that the main surface functions present on our *Canarium Schweinfurthii* cores are carbonyl groups (aldehydes), ethers and -O-H of water or carboxylic acids. These groups are similar to those found on some agricultural lignocellulosic residues [30]. We note a broad absorption band observed between 3600-3300 cm^{-1} with a maximum of around 3400 cm^{-1}. This band is characteristic of the hydrogen elongation vibration of hydroxyl groups (of carboxyl, phenols or alcohols) and of water absorbed by the analyzed materials. The bands observed at 2900 cm^{-1} are absorption bands attributed to the asymmetric and symmetric valence vibration of the -CH_3 group. The bands observed at 1700 cm^{-1} and 1600 cm^{-1} are caused by the elongation vibration of C=O in the ketone, aldehyde, lactone, carbonyl and aromatic ring groups, respectively. This indicates the formation of carbonyl-containing groups. The bands from 1470 to 1370 cm^{-1} are a domain that is formed by an overlap of absorption bands attributable to hydroxyl-type moieties on the surfaces and in-plane vibrations of the C—H bond in several C=C-H structures. The bands between 1000-500 cm^{-1} are due to the out-of-plane CH deformation mode in differently substituted aromatic rings. The presence of the hydroxyl group of the phenolic function and the carboxyl function provides the surface of the materials with an acidic character, while the carbonyl function gives a basic character to the surface of the materials. We notice that the main surface functions present on our *Canarium Schweinfurthii* precursor, are the carbonyl groups (aldehydes), ethers and (-OH) of water or carboxylic acids.

On the other hand, weak bands observed at around 1650 cm^{-1} in CSAC are caused by the elongation vibration of C=O in the ketone, aldehyde, lactone, carbonyl and aromatic ring groups, respectively. This indicates the formation of carbonyl-containing groups. The bands from 1070 to 1370 cm^{-1}(Weak) is a domain that is formed by an overlap of absorption bands attributable to the C-O bond and also to that of the P-O and P=O on the surfaces and in-plane vibrations of the C—H bond in several C=C-H structures. The disappearance of the –OH and other functional groups from the precursors to the carbons indicates the added role of the activating agent (H_3PO_4).

Scanning Electron Microscopy (SEM) Coupled with Energy Dispersive X-ray Spectroscopy (EDX) of CS and CSAC Samples

Scanning Electron Microscopy analysis allows us to visualize the pores of *Canarium Schweinfurthii* (CS) and CSAC. This analysis was performed in order to visualize the surface morphology of the different samples. The results obtained at different resolutions and magnifications are presented in the following **Figure 4**:

SEM Images and EDX of CS and CSAC:

In order to determine the surface morphology and elemental composition of CS and CSAC was performed. **Figure 4** shows the SEM of CS and CSAC at different resolutions and magnifications.

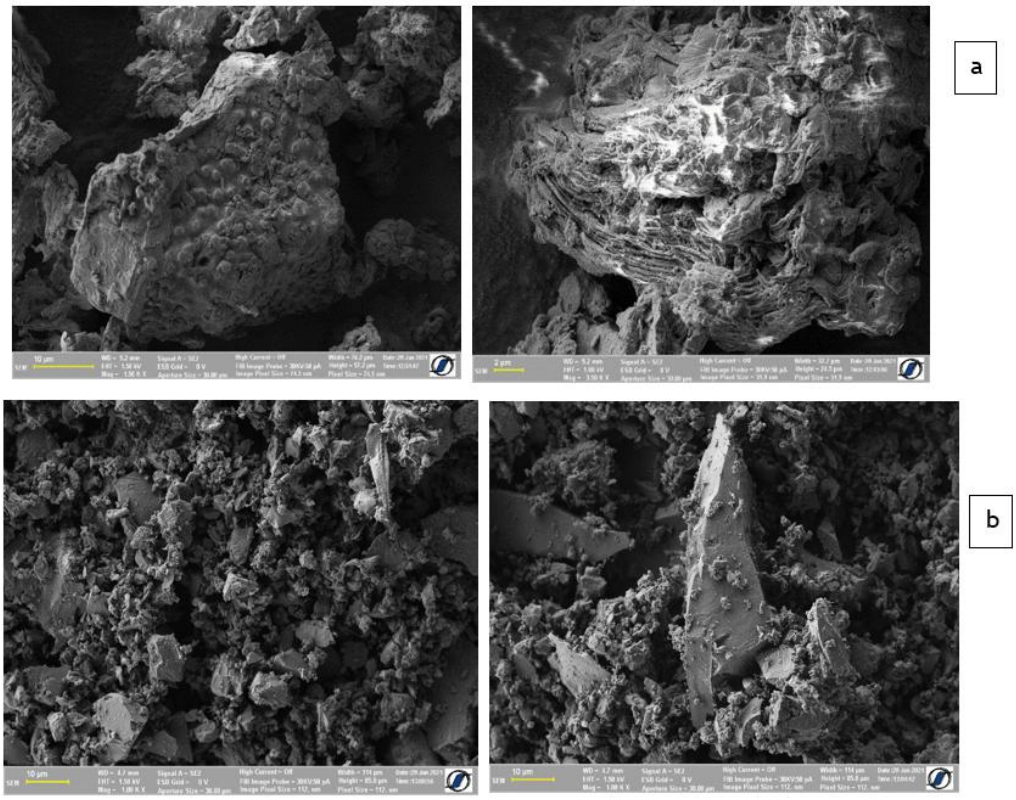

Figure 4: SEM images of CS (a) and CSAC (b) at different resolutions

It follows from Figure 4 (a) it is observe that the surface of *Canarium schweinfurthii* is rock-like with few or no pores. This surface is very rough and shows cracks at high resolutions (10 and 20 µm). The images show a material with a uniformly identical texture with almost no pores. In fact, the pores are less visible. In the case of CS coal (Figure 4b), pores are observed in the form of hairline cracks. These cracks are of different sizes and inside the larger ones we see other cracks of smaller diameter. This observations are in agreement with the results of the BHJ analysis because for adsorption to take place in the micropores and mesopores, the adsorbate must pass through the macropores to reach them [31].

Energy Dispersive X-ray Spectroscopy (EDS)

To obtain the elemental composition of some areas of the micrograph obtained by scanning electron microscopy, two areas were chosen as shown in Figure 5.

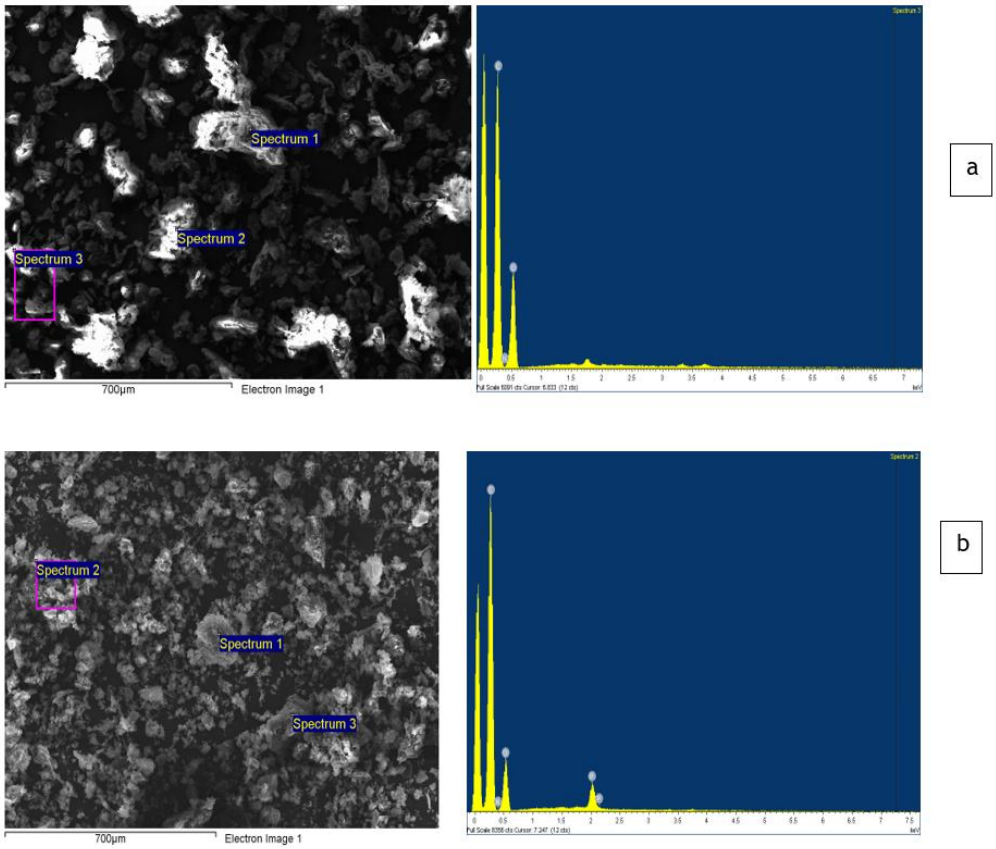

Figure 5: SEM and EDX image of CS (a) and CSAC (b)

It results from Figure 5 (a) that the most abundant element is carbon with an average atomic percentage of 63.28 (Spectrum 1 = 65.41; Spectrum 2 = 64.60 and Spectrum 3 = 59.85), followed by oxygen with an average atomic percentage of 29.23 (Spectrum 1 = 27.96; Spectrum 2 = 27.21 and Spectrum 3 =32.53) plus nitrogen with an average atomic percentage of 7.32 (Spectrum 1 = 6.65; Spectrum 2 = 7.70 and Spectrum 3 =7.62). While magnesium, silicon, potassium and calcium are in trace amounts. The difference in the percentages of the elements in the selected areas and the absence of magnesium, silicon and calcium shows that the atomic dispersion in our samples is not homogeneous. Moreover, the white parts on the CS micrograph give an idea of the fact that we can have a certain degree of crystallinity in our materials. The analysis shows that the CSAC is constituted mainly of carbon atoms and contains oxygen. The highest percentage is that of carbon. This result confirms that activated carbons are strongly carbonaceous materials. The other atoms, phosphorus and nitrogen, are either from the composition of the starting precursors or from the activating agent.

Determination of the pH of the Point of Zero Charge (pH_{PZC}) of the CSAC

The point of zero charge (PZC) of the CSAC sample was studied in this series of pH experiments. The pHpzc of an adsorbent refers to the pH level at which the surface of the adsorbent has zero net charge or the point at which the quantity of the acidic groups is equals that of the basic groups. The pHpzc of the CSAC in this work was determined using

the solid addition/ pH drift method. **Figure 6** presents the change in pH (ΔpH) plotted against the corresponding initial pH values (pHi) for the three adsorbents. The point at which the curves cut the pH axis is taken as the pH_{PZC} of the sample.

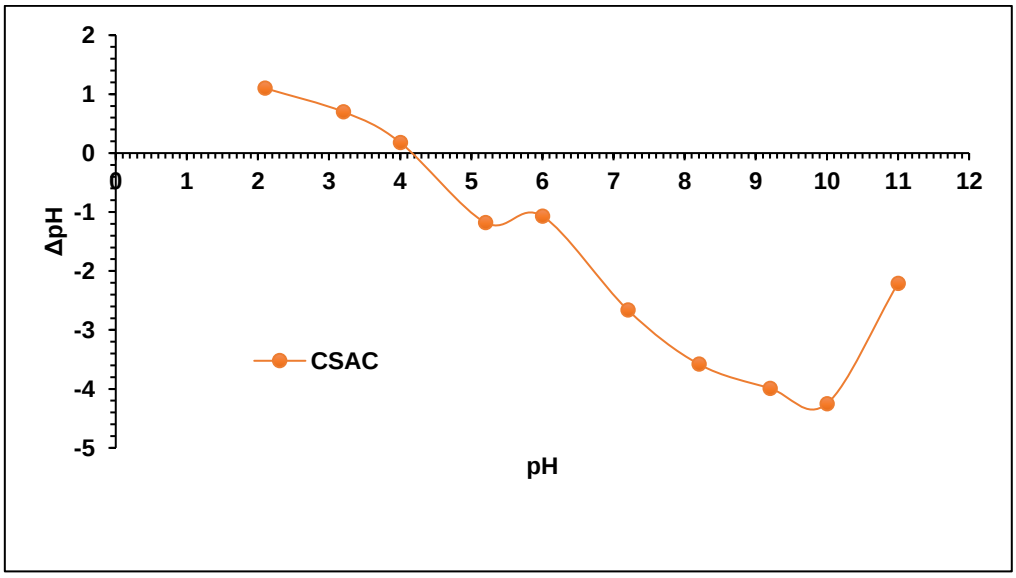

Figure 6: pH of point of zero charge (pH_{PZC}) of CSAC

From Figure 6, the pH_{PZC} of the CSAC was 4.2, and this implies that the CSAC adsorbent surface is acidic in nature, i.e. the surface of the adsorbent contains mostly acidic functional groups. This implies that, during adsorption studies, below the pH_{PZC} value, the surface of the activated carbon is charged positively, while above this value, the surface is positively charged. Also, at the pH_{PZC} value, the net charge on the surface of CSAC material is zero and above 4.2, the net charge of the surface is negatively charged.

Textural Properties of CSAC

The porous nature of these solids is carried out by the drawing of adsorption isotherms which provide important qualitative information on the structure of these materials, illustrated by the shape of the adsorption isotherm relating to these (porosity, diameter and size of the pores). The determination of the surface properties of CSAC was obtained by N_2 adsorption-desorption. The Brunauer–Emmett–Teller (BET) surface area and the pore structure analysis were conducted on a Micromeritics surface Analyzer (Quantachrome, NOVA 1000e series, USA). The pore size distributions were calculated by the density functional theory (DFT) method. It also allows us to have an idea of the specific surface, which is the number of available sites accessible to the molecules on the whole surface of a material.

The texture properties of the CSAC are summarized in **Table I.** The carbon presents a high specific surface area of 1427.000 m^2 g-1 and a large pore volume of 0.4313 ccg^{-1}. The large specific surface area and pore volume could be beneficial for the adsorption of large molecules like dyes, which are large molecules. The pore diameters for the analyzed sample from the DFT result is 1.543 nm suggesting a dominant mesoporosity for the CSAC material.

This implies that, the comments mentioned for the increase in pore volume can also be made for the pore diameter.

Table I: Summary table of the specific surface area, pore diameter and pore volume of the prepared samples

Paramètres	Methods	CSAC
Specific Surface area (mg/g)	BET multi point	1427.000
	BJH method cumulative desorption surface area	343.400
	DH method cumulative desorption surface area	347.600
	DFT cumulative surface area	953.1
pore Volume (cc/g)	BJH method cumulative desorption pore volume	0.4313
	DH method cumulative desorption pore volume	0.4201
	HK method micropore volume	0.5864
	SF method micropore volume	0.3803
	DFT method cumulative pore volume	0.9274
pore Diametre (nm)	BJH method desorption pore Diameter	3.819
	DH method desorption pore Diameter	3.819
	HK method pore Diameter	0.3675
	SF method pore Diameter	0.4523
	DFT pore Diameter	1.543

UV-Vis Analysis of AgNP

The reduction of the pure Ag+ ions was monitored by measuring the reaction medium's UV-Vis spectrum. The UV-Vis spectral analysis was conducted using a UV-Vis spectrophotometer between 300 and 1100 nm. **Figure 7** presents the analytical results obtained for the silver nanoparticles.

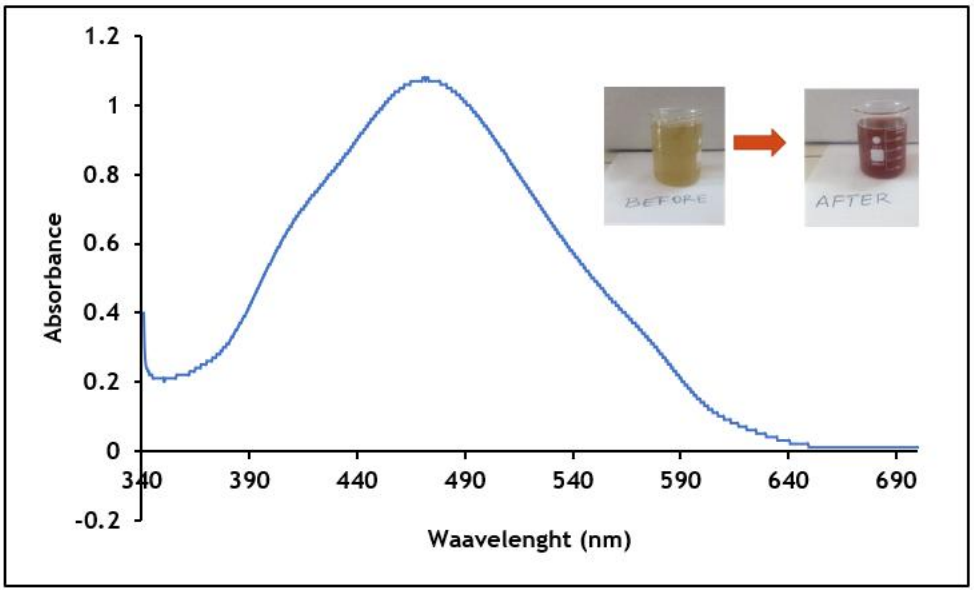

Figure 7: UV-Vis analysis of *Canarium schweinfurthii* synthesized Ag NPs

The Canarium schweinfurthii nut shell extract was slowly introduced into the AgNO3 solution. Initially, it was observed that the orange-clear solution was rapidly changed into dark brown, indicating the formation of AgNPs. No colour change was observed for the AgNO3 solution in the absence of shell extract and equally, no colour change was seen for the shell extract in the absence of the AgNO3 solution. The colour change is an indication of the reduction of Ag+ into Ag0 [32]. Furthermore, the optical UV-Vis analysis of the AgNPs produces a strong and sharp peak observed at 471 nm, which characterised the surface plasmon resonance (SPR) phenomenon [17,32] that confirmed the synthesis of AgNPs attributed to spherical nanoparticles of phenol. Past studies suggested that a surface plasmon resonance (SPR) peak located between 410 and 460 nm has been observed for AgNPs and might be attributed to spherical nanoparticles phenol [17]. The symmetrical shape of the UV-Vis absorption peak indicates the small and uniform size of the anchored Ag nanoparticle

Adsorption Studies Results

Effect of pH

The effect of pH on MO dye adsorbed quantities was investigated under the conditions of 30 min of contact, adsorbent dose of 0.02 g and initial concentration of 100 mg/L on CSAC adsorbent.

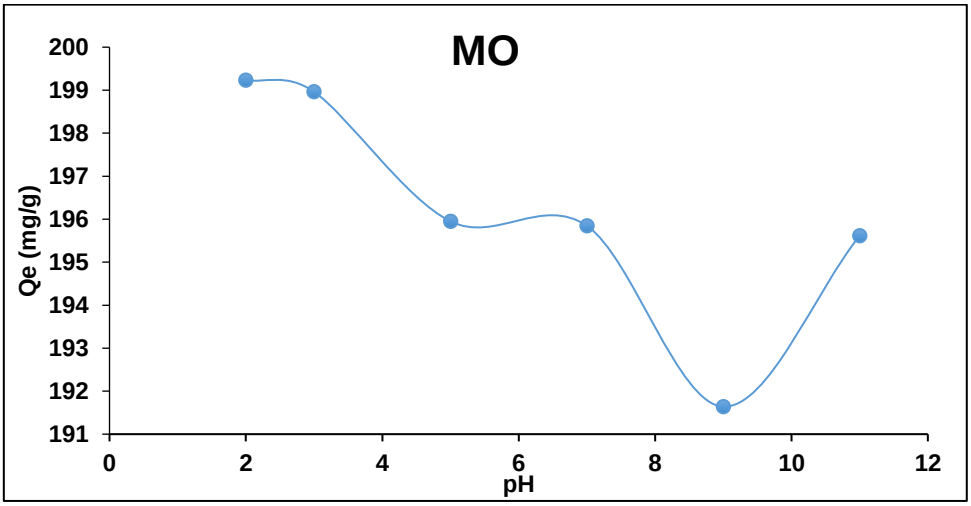

Figure 8: Graph of the effect of pH on MO dye removal onto CSAC adsorbent

According to **Figure 8**, It can be observed that the quantity of MO dye adsorbed on the surface of CSAC material decreases as pH increases. This may be due to the fact that an increase in pH values contributes to an increase in hydroxide ions (OH-) in the solution. These hydroxide ions neutralized the positive sites on the surface of the CSAC material, which does not favour adsorption as there will be electrostatic repulsion with anionic MO dye. However, as the pH decreases, the quantity of MO retained on the CSAC material increases. This might result from the excess H^+ ions protonating the surface of CSAC by neutralizing the negative charges. This favours strong electrostatic attraction between the negative MO dye and the positive CSAC adsorbent. The maximum adsorption quantity is obtained at a lower pH of 2. It is generally known that anionic dyes like MO are preferentially

adsorbed by the adsorbents at lower pH resulting from electrostatic attraction between MO ions and positive adsorbents, which makes adsorption favourable leading to the increasing of adsorbed quantity [17].

Effect of Contact Time

The effect of contact time on MO dye removal onto CSAC is represented in **Figure 9**. The effect of contact time on MO dye adsorption was done at pH 2, MO dye concentration of 100 mg/L and adsorbent dose of 0.02 g at variable times between 0 to 60 min.

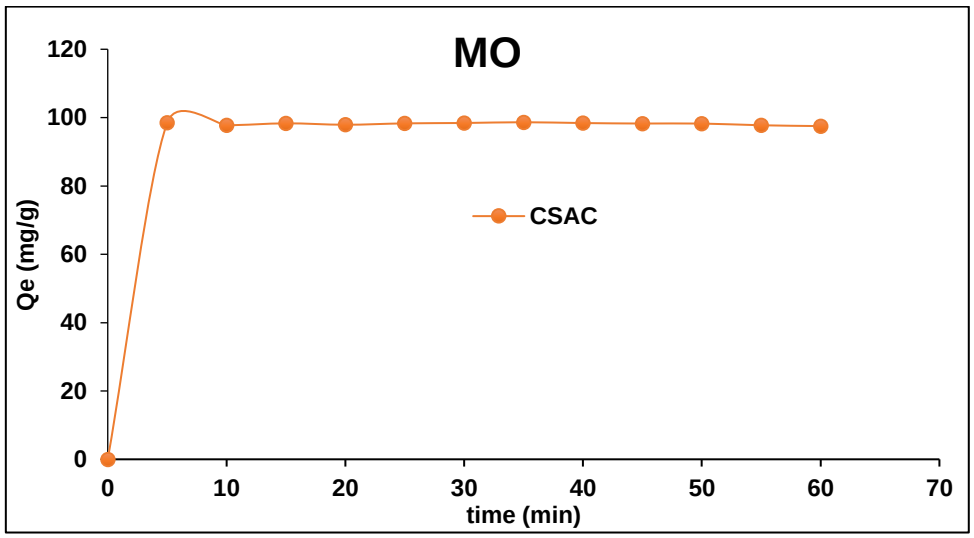

Figure 9: Graph of the effect of contact time on MO dye removal onto CSAC adsorbent

The result from **Figure 9** reveals that, the rate of adsorption is faster within 0 to 5min of the adsorption process. Then, it slows down leading to an equilibrium state. The rapid increase of the MO dye adsorbed quantity during the initial time of the adsorption process may be attributed to the availability of a large number of adsorption sites. It slows down and the establishment of equilibrium within 10 min is due to the saturation of adsorption sites [17]. The adsorbed quantity at equilibrium was **98.168** mg/g. This high amount of retained dye molecules on the surface of the CSAC sample can also result from its large specific surface area and pore size distribution, which makes it favourable for liquid phase adsorption of organic pollutants such as MO dye in terms of both efficiency and economic consideration.

Effect of Adsorbent Dose

The effect of the adsorbent dose on MO dye adsorption for the sample was investigated at pH 2 with an initial concentration of 100 mg/L, and the adsorbent dose varied from 0.01 to 0.06 g and for a contact time of 10 min. Figure 10 displays the results obtained.

Figures 10 show the MO dye adsorbed quantity versus the mass of prepared adsorbent under the optimum conditions. It is seen that MO dye adsorption decreases with an increase in adsorbent dose. Similar results were observed by. The rate of the decrease is more prominent at higher amounts of adsorbate concentration. Significant MO dye

adsorption is achieved for an adsorbent dose of 0.01 g. This observation may be due to the fact that, at lower adsorbent dose, the adsorption sites are available, while at higher adsorbent dose, there is an agglomeration of adsorbent particles, leading to particle size aggregation reducing the available specific surface area and the increased in the diffusional path length [28].

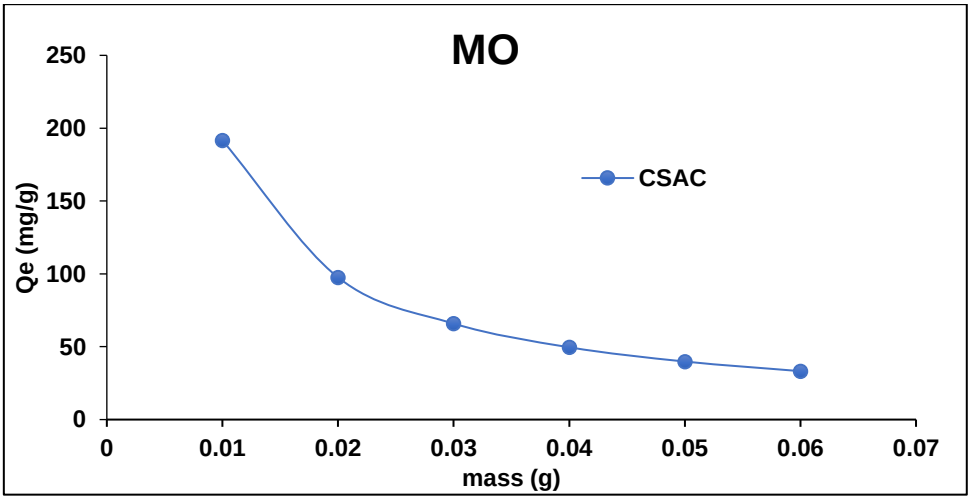

Figure 10: Graph of the effect of adsorbent dose of MO dye removal onto CSAC

Effect of Initial Concentration

The variation of MO dye initial concentration was carried out in the range of 50 to 100 mg/L at the same pH as in the contact time variation, with an adsorbent dose of 0.02 g and the same contact time as in the adsorbent dose variation, respectively. Figure 11 exhibits the MO dye adsorbed quantity for the three adsorbents.

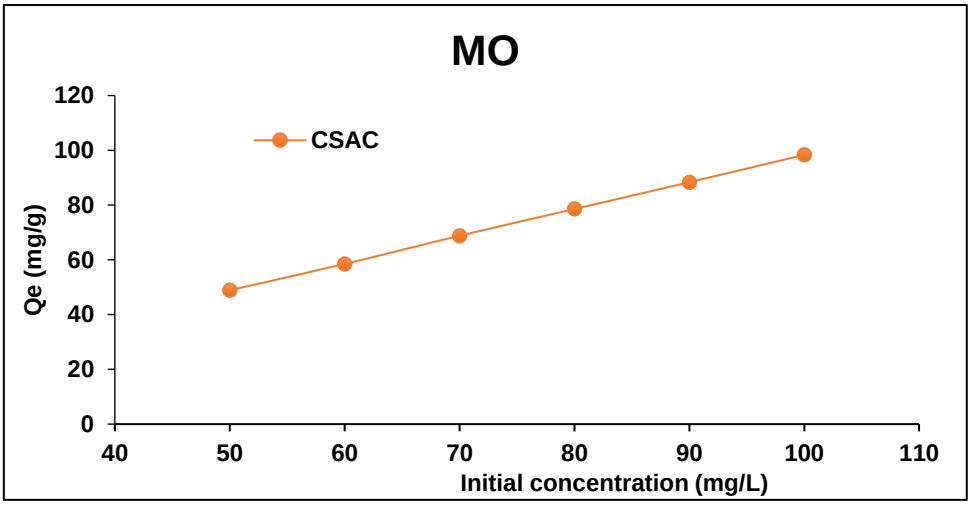

Figure 11: Graph of the effect of initial concentration of MO dye removal onto CSAC

The results showed that as the initial concentration of the MO dye increases, the adsorbed quantity per unit of adsorbent mass also increases. The adsorbed quantity varies

from MO dye, it varies from 48.293 to 98.328 mg/g of CSAC material. The increase in adsorbed quantity is mainly due to the increase of effective collisions in solution between the MO dye molecules on the respective adsorbents. This increase in effective collision decreases the activation energy of the colliding particles which helps to overcome the mass transfer resistance between the aqueous and solid phases [17, 28]. This decrease in activation energy favours the adsorption of MO dye adsorption onto the respective adsorbents.

Non-linear Adsorption Isotherms and Kinetic Modelling

Non-Isotherm Studies of MO dye onto CSAC Adsorbent

The plots of three isotherm models for MO dye adsorption onto CSAC are presented in Figure 12, and their calculated values parameters are reported in Table II.

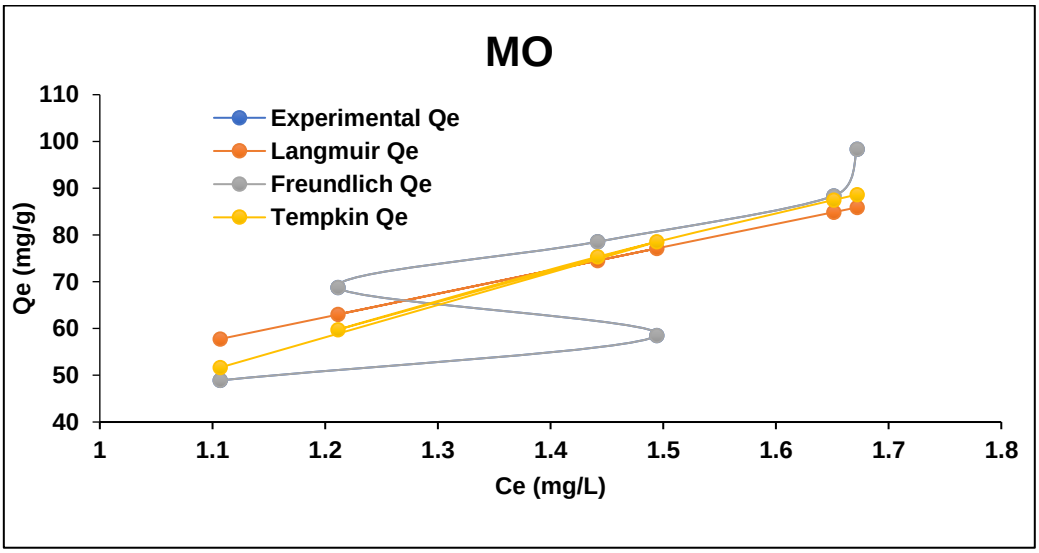

Figure 12: Representation of the nonlinear isotherm models plot for CSAC adsorbent on MO dye adsorption

Langmuir adsorption isotherm is best known for its applicability to explain the adsorption phenomenon on monolayer coverage, hence predicting a chemisorption process with strong forces between the adsorbate and the adsorbents. From Table II, the Langmuir for the three adsorbents and MO dye adsorption could not completely elucidate the adsorption phenomenon due to their low correlation coefficient. That notwithstanding, the Langmuir separation constant RL is found between 0 and 1 (i.e. 0 < RL < 1), implying the adsorption of the two adsorbates on the respective adsorbents is favourable.

The Freundlich isotherm model which is best applies to adsorption on heterogeneous surfaces with interaction between the adsorbed molecules and there is no restriction to the formation of a multi-layer best fitted the adsorption of MO onto CSAC adsorbent with respect to its R^2 values of unity (1.000). Also, the high value of the Freundlich constant (KF) makes the model applicable to presume there is the possibility of the formation of a multi-layer coverage on the surface of the respective adsorbents at higher dye concentrations. This

possibility was further strengthened by the low values of *RMSE* and x^2 for both adsorbates on all the respective adsorbents. In addition, Freundlich heterogeneity factor *1/n* is 1 implying that the surface of the CSAC adsorbent is homogenous vis-à-vis the MO adsorbate.

Table II: Summary Table of the different relative isotherm constants and their respective determination coefficients (R^2. *RMSE* and x^2) for the adsorption of MO

Isotherm models	Parameters	CSAC Adsorbent
Langmuir	q_m (mg g^{-1})	1860.792
	K_L (L. g^{-1})	0.029
	R^2	0.626
	RMSE	12.663
	x^2	23.891
	R_L	0.409
Freundlich	K_F (L. g^{-1})	1.000
	1/n	1.000
	R^2	1.000
	RMSE	$2.349*10^{-6}$
	x^2	$4.361*10^{-13}$
Tempkin	A_T (L. g^{-1})	1.609
	B_T (J. mol^{-1})	27.663
	R^2	0.653
	RMSE	12.206
	x^2	7.833

The Tempkin Isotherm model is used to explain the adsorption phenomenon because it contains a factor that explicitly takes into account the adsorbent–adsorbate interactions by ignoring the extremely low and large value of concentrations, the model assumes that heat of adsorption (function of temperature) of all molecules in the layer would decrease linearly rather than the logarithmic with coverage [33]. According to **Table II**, the Tempkin isotherm on MO dye adsorption could not completely elucidate the adsorption phenomenon due to its low correlation coefficient.

Kinetics Studies of the Adsorption of MO Dye on CSAC Adsorbent

The kinetic curves are shown in Figure 13 while their kinetic parameters are gathered in Table III.

From **Table III**, the pseudo-first kinetic and pseudo-second-order model best fitted the adsorption of MO on CSAC based on their high correlation coefficient of unity. Also, their experimental quantity adsorbed, which is close to the theoretical quantity adsorbed at equilibrium, confirms the validity of this model on the above respective adsorbent. Also, the low values of *RMSE* and x^2 for both the pseudo-first and pseudo-second-order kinetic models add to the credibility of the model in explaining the adsorption mechanisms of MO on the adsorbents. This suggests competition between physical and chemical adsorption of MO dye on CSAC adsorbent.

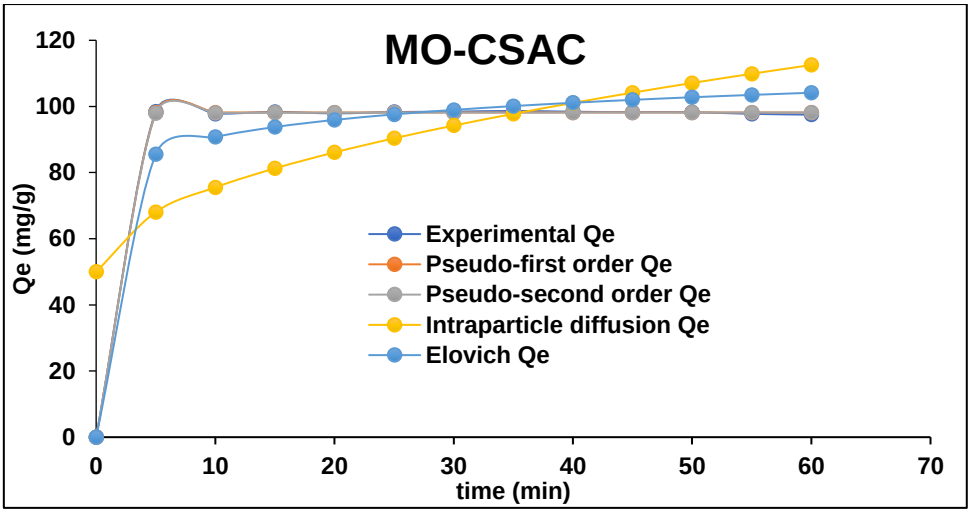

Figure 13: Representation of the nonlinear kinetic models plot for CSAC adsorbent for MO dye adsorption

Table III: Summary table of Correlation coefficients and non-linear constants of kinetic models on the Adsorption Kinetics of MO on CSAC adsorbent

Kinetic models	Parameters	CSAC Adsorbent
	q_e (exp) (mg g^{-1})	**98.464**
Pseudo-first order	q_e (pred) (mg g^{-1})	98.196
	k_1 (min^{-1})	2.481
	R^2	1.000
	RMSE	0.345
	x^2	0.013
Pseudo-second order	q_e (pred) (mg g^{-1})	98.187
	K_2 (mg $g^{-1}min^{-1}$)	0.0.724
	R^2	1.000
	RMSE	0.369
	x^2	0.015
Intra-particle diffusion	k_{id}	8.073
	C_i (mg. g^{-1})	50.002
	R^2	-0.239
	RMSE	21.157
	x^2	80.709
Elovich	α (mg $g^{-1}min^{-1}$)	138399.374
	β (g. min^{-1})	0.134
	R^2	0.961
	RMSE	5.741
	x^2	3.936

With respect to R^2 values, the Intra-particle diffusion model is not the most suitable to explain the adsorption of MO on CSAC adsorbent because of its negative constant of negative R^2 value. However, the large values of the diffusion constant value K_{id} for the model implies that the diffusion rate of MO is important in the adsorption process; but that notwithstanding, the high values of the constant C_i (which is the repulsion barrier between the adsorbate and the adsorbent) for all the adsorption processes of MO on CSAC is an

indication that the intra-particle diffusion step is not the rate-limiting step in the adsorption mechanism.

In the case of the Elovich model, the R^2 value for MO dye adsorption onto adsorbent was significant (R^2=0.961). Also, the *RMSE* and x^2 values, which were respectively low at higher concentrations, throw further significance of this model to explain the adsorption of MO dye on CSAC adsorbent. Nevertheless, The Elovich adsorption speed constant (*a*) is far greater than the desorption coefficient *β* which strongly declares without any doubt or fear of uncertainty that the adsorption process of MO on CSAC adsorbent is dominated by chemisorption.

Anti-microbial Result of the Samples *Escherichia coli*, *Staphylococcus aureus*, *Staphylococcus aureus*, and Salmonella Serovars

The microbial growth inhibition capacities of the AgNPs prepared from CS aqueous extract and CSAC/AgNP material were assessed using Minimum Inhibitory Concentration (MIC) and Minimum Bactericidal Concentration (MBC). The experimental MIC and MBC results are grouped in Table IV.

Table IV: Antibacterial activity of the obtained materials

Minimum Inhibitory Concentration (MIC) and Minimum Bactericidal Concentration (MBC) in (µg/ml)							
Samples	**Parameters**	**EC ATCC 25922**	**SA ATCC 43300**	**SANR 46003**	**S.Cho NR 170**	**SE NR 13555**	**SE NR 4811**
CS Extract	MIC	>1000	>1000	>1000	>1000	>1000	>1000
	MBC	>1000	>1000	>1000	>1000	>1000	>1000
CSAC	MIC	>1000	>1000	>1000	>1000	>1000	>1000
	MBC	>1000	>1000	>1000	>1000	>1000	>1000
NPS	MIC	7.812	31.25	31.25	31.25	31.25	62.5
	MBC	7.812	250	31.25	31.25	31.25	125
CS	MIC	31.25	125	125	31.25	62.5	250
	MBC	31.25	1000	250	500	125	250
Ciprofloxacin	MIC	0.031	0.078	0.078	0.153	3.9062	0.078

EC ATCC25922: Escherichia coli ATCC25922; SA ATCC43300: Staphylococcus aureus ATCC 43300; SANR 46003: Staphylococcus aureus NR 46003; S.cho NR-170: Salmonella choleriesus NR-170; SENR 13555: Salmonella enteritica 13555; SENR 4811: Salmonella enteritica 4811

The MIC values range from 7.782 µg/mL to 31.25 µg/mL for Escherichia coli, Staphylococcus aureus, Staphylococcus aureus, Salmonella choleriesus, Salmonella enteritica and 62.5 µg/mL for Salmonella enteritica in the case of the AgNPs. For the CSAC/AgNP sample, it ranges from 31.25 µg/mL to 125 µg/mL for Escherichia coli, Staphylococcus aureus, Staphylococcus aureus, Salmonella choleriesus, Salmonella enteritica and 250 µg/mL for Salmonella enteritica. The activated carbon doped with silver nanoparticles is slightly less active than the simple nanoparticles alone. The results equally showed that Escherichia coli, Staphylococcus aureus, Staphylococcus aureus, Salmonella choleriesus, Salmonella enteritica and 62.5 µg/mL are more susceptible to destruction than

Salmonella enteritica. The un-doped activated carbon and the extract showed no activity against any of the strains at the tested concentrations. According to [34], the antimicrobial activity of a plant extract is considered to be highly active if the MIC < 100 µg/mL; significantly active when 100 ≤MIC ≤512 µg/mL; moderately active when 512 <MIC ≤2048 µg/mL; weakly active if MIC > 2048 µg/mL and not active when MIC >10 000 µg/mL. However, to the best of our knowledge, no such classification exists for solid carbons, doped carbons and nanoparticles materials. Interestingly, these samples exhibited high antibacterial activities (MIC < 100) with respectct to the above classification. Furthermore, all the MBC of the AgNP (CSAC/AgNP and AgNP) are equal to their respective MIC while that of the CSAC/AgNP are is higher than that of the MIC. These implies that the nanoparticles have a bactericidal effect while the composite have bacteriostatic effect with respect to the studied bacteria.

CONCLUSION

Generally, CSAC, Green silver nanoparticles, CSAC/AgNP materials have been introduced and specifically designed with the aim of targeting bacterial contaminated water. Water polluted by dyes and water containing bacteria were the prime suspect. The CSAC material prepared from Canarium schweinfurthii shells was prepared for dyes containing water and tested on MO dye removal in aqueous solution. The adsorption results obtained are consistent and have shown high adsorption capacities greater than 99% of dye removal. The FT-IR spectra of CSAC shows a drastic modification in the different surface functional groups from the CS precursor to the carbon and was confirmed by the SEM-EDS analysis showing high percentage of carbon in CSAC. The N2 adsorption-desorption isotherm according to BET method shows higher specific surface area, pore volume and pore diameter for CSAC. The strength of the pore capacity and surface functional group of the prepared samples were unmasked on the retention of MO dye from aqueous solution. The amount of MO dye uptake on the CSAC varied from 48.293 to 98.328 mg/g. The isotherm and kinetic modeling of the experimental data using non-linear regression shows that, Freundlich isotherm model, pseudo-first and pseudo-second order kinetic model gave the best fit to explain the adsorption equilibrium and mechanism for the adsorbent. It was also found that the MO dye adsorption mechanism was dominant chemisorption with higher adsorption speed constant (α) of the Elovich kinetic model. The AgNP prepared from aqueous extract of Canarium schweinfurthii shells and CSAC/AgNP material was prepared for bacteria containing water and tested on six bacteria isolates of EC ATCC25922: Escherichia coli ATCC25922; SA ATCC43300: Staphylococcus aureus ATCC 43300; SANR 46003: Staphylococcus aureus NR 46003; S.cho NR-170: Salmonella choleriesus NR-170; SENR 13555: Salmonella enteritica 13555; SENR 4811: Salmonella enteritica 4811 gotten from the 'Centre Hospitalier Universitaire' (CHU) of Yaounde-Cameroon. From Tamokou's classification, the AgNP and CSAC/AgNP exhibited high antibacterial activities (MIC < 100) and the AgNP had bactericidal effect with respect to the chosen strain. Therefor AgNP introduction into CSAC will make the CSAC material to possess double function as it will efficiently eliminate dyes and exhibit strong antimicrobial property to the filters while preserving its adsorption characteristics. Furthermore, this process could be scaled up easily for the industrial applications to increase the yield of the nanoparticles significantly since Canarium schweinfurthii nut shells are primordially considered as potential waste, which undoubtedly would establish its commercial viability in medicine.

ACKNOWLEDGMENTS

Authors gratefully acknowledge Dr. George STOIAN of the National Institute of Research and Development for Technical Physics-NIRDTP Iasi, Romania for HR-SEM images and EDX measurements and Dr. Rami A DOUKEH from the Faculty of Petroleum Technology and Petrochemistry, Petroleum and Gas University of Ploiesti Romania for logistics facilities.

REFERENCES

[1] Abdulrahman A-N, Ahmed A, Gordon M, (2021) Removal of phenols and dyes from aqueous solutions using graphene and graphene composite adsorption: A review. J Envl Chem Eng 9, 1-15. https://doi.org/10.1016/j.jece.2021.105858

[2] Tekin D, Birhan D Kiziltas H, (2020) Thermal, Photocatalytic, and antibacterial properties of calcinated nano-TiO2/polymer composites, Mater Chem and Phy. doi: https://doi.org/10.1016/j.matchemphys.2020.123067.

[3] Paiva de Freitas F, Ana Mcia Macedo Ladeira Carvalho,Angélica de Cássia Oliveira Carneiro, Mateus AM, Mariana FX, Wagner DC (2021), "Adsorption of neutral red dye by chitosan and activated carbon composite films", Heliyon, 7, 1-10. https://doi.org/10.1016/j.heliyon.2021.e07629

[4] Marrakchi F, Bouaziz, M Hameed BH (2017) Activated carbon–clay composite as an effective adsorbent from the spent bleaching sorbent of olive pomace oil: Process optimization and adsorption of acid blue 29 and methylene blue. Chem. Eng. Res. Des., 1-34, https://doi.org/10.1016/j.cherd.2017.10.015.

[5] Ghorbani M, Salem S, (2020) Solar treatment of sewage discharged from industrial estate for reduction of chemical oxygen demand over Degussa P-25 titania. Chemosphere, https://doi.org/10.1016/j.chemosphere.2020.129123

[6] Arminda, M., Josúe, C., Cristina, D., Fabiana, S., & Yolanda, M. (2021). Use of activated carbons for detoxification of a lignocellulosic hydrolysate: Statistical optimisation. Journal of environmental management, 296, 113320.

[7] Yuan P, Ding X, Gao N, Zhu H, Yi YY, Xu Q-H (2016) Au-Ag Core-shell Nanoparticles for Simultaneous Bacterial Imaging and Synergistic Antibacterial Activity,Nanomedicine: Nanotech, Bio, and Med, doi: 10.1016/j.nano.2016.09.003

[8] Solmaz A, Esra DA, Muzaffer Y Oray E (2013) The Effect of Ag Content of the Chitosan-Silver Nanoparticle, Composite Material on the Structure and Antibacterial Activity. Adv Mater Sci and Eng. 1-7. http://dx.doi.org/10.1155/2013/690918

[9] Nithya P, Balaji M, Mayakrishnan A (2019) Ionic liquid functionalized biogenic synthesis of Ag-Au bimetal doped CeO2 nanoparticles from Justicia adhatoda for pharmaceutical applications: Antibacterial and anti-cancer activities. J Photochem & Photobiol, B: Biology, https://doi.org/10.1016/j.jphotobiol.2019.111706

[10] Fiori-Duarte AT, Paiva REF., Manzano CM, Lustri WR, Corbi PP (2020) Silver(I) and gold(I) complexes with sulfasalazine: Spectroscopic characterization, theoretical studies and antiproliferative activities over Gram-positive and Gram-negative bacterial strains, J. Mol.Strct. doi: https://doi.org/10.1016/j.molstruc.2020.128158.

[11] Tianyu L, Qianyue P Kang M, Xiaoting H, Li X, Feiyan Z, Yi L (2022) Silver nanoparticle@carbon quantum dot composite as an antibacterial agent. RSC, 12, 9621-9627. DOI: 10.1039/D2RA00561A

[12] Shakeel AK, Sammia S, Chun-Sing L (2020) Using Leaf Extract of Clerodendrum inerme; Characterization, Antimicrobial, and Antioxidant Activities. Biomol. 10, 835.

[13] Arockia JD, Sathyavathi K, Umadevi M, Parimaladevi R, (2019) Enhanced bioactivity of Fe3O4-Au nanocomposites- A comparative antibacterial study, Materials Letters. doi: https://doi.org/10.1016/j.matlet.2019.126795

[14] Wang M, Xie R, Chen Y, Pu X, Jiang W, Yao L (2018) A novel mesoporous zeoliteactivated carbon composite as an effective adsorbent for removal of ammonia-nitrogen and methylene blue from aqueous solution. Bioresour. Technol., 1-35, doi: https://doi.org/10.1016/j.biortech.2018.08.037.

[15] Nasim A Azadeh T (2019) Adsorption of Rhodamine-B from Aqueous Solution by Activated Carbon from Almond Shell. Proc., 41(51), 1-4, doi: 10.3390/ecsoc-23-06619.

[16] Kouotou D, Mohammed G, Ndi JN, Luisa MPM, Meriam El O, Ketcha JM, and El Khadir G (2021a) Removal of metallic trace elements (Pb2+, Cd2+, Cu2+ and Ni2+) from aqueous solution by adsorption onto cerium oxide modified activated carbon. Environ. Monit. Assess., 193(467).

[17] Ankoro NO, Kouotou D, Lunga P K, Agbor GT, Lekene NR, Ndi JN, Ketcha JM (2020) Effect of Doping Activated Carbon Based Ricinodendron Heudelotti Shells with AgNPs on the Adsorption of Indigo Carmine and its Antibacterial Properties. Arab. J. Chem., 13, 5241–5253, https://doi.org/10.1016/j.arabjc.2020.03.002.

[18] Jyoti, S, Garg, VK, Gupta, RK, Navish K (2017) Removal of Orange G and Rhodamine B dyes from aqueous system using hydrothermally synthesized zinc oxide loaded activated carbon (ZnO-AC). J. Environ. Chem. Eng. http://dx.doi.org/10.1016/j.jece.2017.01.012.

[19] Lili D, Bo Z, Wei G, Qi L, Zichen W, Yupeng G, Xiaofeng W, Yanhua L, (2014) Adsorption of Rhodamine-B from aqueous solution using treated rice husk-based activated carbon. Colloids Surf A: Physicochem. Eng. Asp., 446, 1–7. http://dx.doi.org/10.1016/j.colsurfa.2014.01.030.

[20] Noppon S, Viboon S, Aht-Ong D, (2020) Adsorption removal of methylene blue onto activated carbon/cellulose biocomposite films: Equilibrium and kinetic studies. Mater. Chem. Phys., 240, 1-14, https://doi.org/10.1016/j.matchemphys.2019.122221

[21] Kouotou, D, Ghalit M, El Ouahabi M Gharibi E, (2021(b)). Removal of formaldehyde and methylene blue from aqueous solution by adsorption on cerium-doped activated carbon: a comparative study. Int. J. Environ. Anal. Chem., doi: 10.1080/03067319.2021.1991335.

[22] Lunhong A, Ming L, Long L (2011) Adsorption of Methylene Blue from Aqueous Solution with Activated Carbon/Cobalt Ferrite/Alginate Composite Beads: Kinetics, Isotherms, and Thermodynamics. Chem. Eng. Data, 56, 3475–3483, dx.doi.org/10.1021/je200536h.

[23] Niyaz MM, Mohsen T and Ali T (2018) Activated carbon/metal-organic framework composite as a bio-based novel green adsorbent: Preparation and mathematical pollutant removal modeling, Molliq. https://doi.org/10.1016/j.molliq.2018.12.050

[24] Kadir Erol, Melda Bolat, Demet Tatar, Cengiz Nigiz, Dursun Ali Köse, (2020), “Synthesis, characterization and antibacterial application of silver nanoparticle embedded composite cryogels”, J. Mol.Strct.1200, 1-8. https://doi.org/10.1016/j.molstruc.2019.127060

[25] Gao L, Wang L, Yang L, Yinghu Z, Nan S, Chongwei A, Youyi S, Jun X, Haibin W, Yali S, Yanling R (2019) Preparation, characterization and antibacterial activity of silver nanoparticle/graphene oxide/diatomite composite. Appl Surf Sci, https://doi.org/10.1016/j.apsusc.2019.04.153

[26] Shiyi F, Feng Z, Saeed A, Yaowen L (2019) Physico-Mechanical and Antibacterial Properties of PLA/TiO2 Composite Materials Synthesized via Electrospinning and Solution Casting Processes. Coatings, 9, 1-17, doi:10.3390/coatings9080525

[27] Arunkumar L, Sangappa KG, Shashidhar (2019) Synthesis, characterization and antibacterial study of Ag–Au Bi-metallic nanocomposite by bioreduction using piper betle leaf extract. Heliyon, 5, 1-6. doi:10.3390/biom10060835

[28] Lekene NRB, Kouotou D, Ankoro NO, Kouoh, SAPM, Ndi JN Ketcha, JM, (2021) Development and tailoring of amino-functionalized activated carbon based Cucumerupsi manni Naudin seed shells for the removal of nitrate ions from aqueous solution. J Saudi Chem Soc, doi: https://doi.org/10.1016/j.jscs.2021.101316.

[29] Ran W, Taotao M, Bowen Z, Chuchu C, Dagang L, (2021) Preparation and characterization of activated carbon/ultra-high molecular weight polyethylene composites. Polym Compo, 1–9, https://orcid.org/0000-0003-4366-3202.

[30] Baquero, M. C., Giraldo, L., Moreno, J. C., Suarez-Garcıa, F., Martınez-Alonso, A., & Tascon, J. M. D. (2003). Activated carbons by pyrolysis of coffee bean husks in presence of phosphoric acid. Journal of analytical and applied pyrolysis, 70(2), 779-784.

[31] Benaddi, H., Bandosz, T. J., Jagiello, J., Schwarz, J. A., Rouzaud, J. N., Legras, D., & Béguin, F. (2000). Surface functionality and porosity of activated carbons obtained from chemical activation of wood. Carbon, 38(5), 669-674.

[32] Al-Ansari M., Alkubaisi N., Gopinath K., Karthika V., Arumugam A. and Govindarajan M., 2019, “Parameters optimization for nitrate removal from water using activated carbon and composite of activated carbon and Fe2O3 nanoparticles”, Journal of Cluster Science, (30),1081–1089, https://doi.org/10.1007/s10876-019-01569-w

[33] Mehrabi N., Soleimani M., Yeganeh M. M. and Sharififard H, 2015, “Parameters optimization for nitrate removal from water using activated carbon and composite of activated
carbon and Fe2O3 nanoparticles”, The Royal Society of Chemistry, 5(64), 51470-51482, DOI: 10.1039/C5RA03920G

[34] Tamokou J. D., Mbaveng T. A., and Kuete V., 2017 “Antimicrobial activities of African medicinal spices and vegetables. In: Medicinal spices and vegetables from Africa: therapeutic potential against metabolic inflammatory infectious and systemic diseases”, 1st edition. Elsevier; p. 207-237.